
Fast and Effective GNN Training with Linearized Random Spanning Trees

Francesco Bonchi^{*}
bonchi@centai.eu

Claudio Gentile[†]
cgentile@google.com

André Panisson[‡]
panisson@centai.eu

Fabio Vitale[§]
fabio.vitale@centai.eu

Abstract

We present a new effective and scalable framework for training GNNs in supervised node classification tasks, given graph-structured data. Our approach increasingly refines the weight update operations on a sequence of path graphs obtained by linearizing random spanning trees extracted from the input network. The path graphs are designed to retain essential topological and node information of the original graph. At the same time, the sparsity of these path graphs enables a much lighter GNN training which, besides scalability, helps mitigate classical training issues, like over-squashing and over-smoothing. We carry out an extensive experimental investigation on a number of real-world graph benchmarks, where we apply our framework to graph convolutional networks, showing *simultaneous* improvement of both training speed and test accuracy, as compared to well-known baselines.

1 Introduction

Graph Neural Networks (GNNs), particularly Graph Convolutional Networks (GCNs) [24] and Graph Attention Networks (GATs) [33], have demonstrated remarkable success in a variety of application domains, including social networks, molecular biology, and computer vision. However, the fundamental message passing operation, intrinsic in most of GNN learning schemes, requires each node to pool data from all neighboring nodes, leading to high computational and memory requirements, which limit their scalability to large-scale graph and applicability in real-world scenarios.

Besides the mere scalability, there are other computational issues that hamper the discriminative power of GNN, such as the so-called *over-squashing* and *over-smoothing* phenomena. Over-smoothing refers to the excessive compression of node features in GNNs during the aggregation phase, causing a loss of discriminative information [6, 28]. In GCNs, for example, features are combined in a weighted manner by averaging neighboring nodes’ features. The problem arises when nodes with different features end up having similar representations after multiple layers of aggregation, making it difficult for the model to distinguish between them. This is particularly problematic when the activation function aggressively compresses the input into a narrow range of output values (e.g., a sigmoid) potentially leading to the “*vanishing gradient problem*”, which makes it difficult to learn useful representations of the input data. Over-squashing [2, 32, 16, 3] occurs when an exponential amount of information is compressed into a fixed-size vector. This compression can result in a loss of

^{*}Centai

[†]Google Research

[‡]Centai

[§]Centai

critical information and degrade the performance of the GNN. The receptive field of a node, which is the region or set of input values that a particular node can process, tends to grow exponentially with each additional layer in the network. This rapid growth often leads to a bottleneck effect, exacerbating over-squashing. Both GCNs and GATs suffer from over-squashing, as they rely on iterative message passing schemes for feature aggregation. In deeper GNNs, over-squashing becomes way more pronounced, as the node representations become increasingly influenced by distant nodes in the graph, which may cause all node embeddings to converge to the same value [2, 32, 16].

Graph Effective Resistance Network (GERN). In this paper, we propose GERN, a GNN-training framework based on a sparsification process that captures relevant graph properties via the *effective resistance* of the edges, which is a powerful tool widely used in the graph-based learning literature – see, e.g., [19, 4, 5, 20, 30, 1, 15, 3]. GERN (presented in Section 3) operates on a sequence of *uniformly generated Random Spanning Trees* (RSTs) of the input graph G , suitably linearized into *Random Path Graphs* (RPGs), and increasingly refining the weight matrix by sharing and updating it during the whole training process. The RPGs are designed to retain essential topological and node information of G . The sparsity of the RPGs enables much lighter GNN training which, besides scalability, helps mitigate classical training issues, like the aforementioned over-squashing and over-smoothing. Our method can also be viewed as a GNN equipped with a *randomized* self-attention mechanism that enables the aggregation of the neighbors of each node based on the graph topology and the strength of the connections, independent of the feature vectors. The randomized node selection relies on a distribution directly related to the effective resistance of the involved edges within the graph. Although our framework is flexible enough to be deployed in several types of GNNs for node classification, in this paper we just focus on a message passing architectures inspired by the classical Graph Convolutional Networks [24]. Our experiments on a number of real-world graph benchmarks (Section 4), confirm that GERN achieves the simultaneous improvement of both training speed and test accuracy, as compared to well-known baselines.

State of the art. Several sampling-based methods have been proposed to reduce the computational and memory burden of GNNs. Among them are the methods described in [18, 36, 8, 7, 22]. GraphSAGE [18] is an inductive learning method that generates embeddings for out-of-sample nodes, by sampling and aggregating features from the node’s neighbors. GraphSAINT [36] uses random node, edge, and subgraph sampling techniques to generate mini-batches for training. It also normalizes the graph data to reduce the variance of the gradient estimate, making the training process more stable and efficient. FastGCN [8] employs importance sampling to select a small subset of nodes for efficient computation of each layer’s approximate gradient. [7] proposes a stochastic training method for GCNs that uses a control variate-based technique to reduce variance in the gradient estimate, and layer-wise sampling for scalability. Finally, [22] introduces an adaptive layer-wise sampling method to speed up the training of GNNs, which dynamically adjusts the number of sampled neighbors in each layer according to their impacts on the final output. We note that none of these sampling techniques is similar to the one exploited by GERN. We will use GraphSAGE [18] and GraphSAINT [36] in our experimental comparison in Section 4.

There are other approaches in the literature aimed at making GNN training more scalable, without resorting to sampling. Cluster-GCN [10] partitions the graph into subgraphs, which are then processed in a mini-batch manner, opening doors to parallelization and thus scalability. Another paper relying on partitioning the input graph is [25], that proposes a scalable semi-supervised learning framework based on partitioning the graph into multiple balanced subgraphs. Each subgraph is then independently processed by a GNN. [9] proposes an ingenious bidirectional propagation method for GNNs. It splits each graph convolution into two half convolutions, one aggregating the information from the neighborhood to the target nodes and the other propagating the information back to the neighborhood. Finally, Sketch-GNN [13] leverages sketching techniques to map high-dimensional data structures into a lower dimension, which is done before training. Specifically, the authors sketch both the adjacency matrix and the node feature matrix of the graph. The sketch-ratio required to maintain “full-graph” model performance drops as the graph size increases, implying that Sketch-GNN can scale sublinearly with the graph size. In this regards, it is worth highlighting that also the generation of each RPG for GERN is sublinear in the number of edges, if we exclude pathological input graphs whose characteristics never occur in real-world scenarios (see, e.g., [34]).

Since the cornerstone of GERN is the random transformation of the input graph into a path graph focused on effective resistance, it is pertinent to cite GraphZoom [12], where a technique is proposed that leverages effective resistance to enhance the scalability and accuracy of graph embeddings.

In particular, GraphZoom relies on effective resistance to decide which nodes to combine into supernodes. Such process aims at preserving the spectral properties of the graph [37], so that the embeddings learned from the coarser graph are also applicable to the original graph. The very recent work [3] provides theoretical evidence that effective resistance can be used as a measure of oversquashing between a pair of nodes, and that the total resistance can be used as a measure of total oversquashing in a graph. Then it studies how to improve the connectivity of a graph through total effective resistance-based rewiring, to enhance the performance of GNNs for *graph classification*.

Summary of our contributions. Our contributions can be summarized as follows.

- (i) We demonstrate the effectiveness of training GNNs where the feature vectors aggregation is *weighted* by the effective resistance of the involved edges.
- (ii) Motivated by scalability concerns, we develop a novel, scalable, and flexible framework for approximating such a weighing scheme via uniformly generated RSTs, suitably linearized into RGPs. In passing, we introduce very fast heuristics for generating RSTs that *approximate* uniformly generated ones, and experimentally validate the accuracy of this approximation. An important property of these RSTs is that they can be generated in parallel during training. We empirically show that, when generating them in parallel, our training framework turns out to be 10-20 times *faster* than competing methods, while almost consistently *outperforming* these methods in test set accuracy on real-world datasets.
- (iii) Our proposal largely mitigates over-squashing and over-smoothing phenomena; this is an important side-effect of operating with path graphs instead of the whole input graph.

2 Preliminaries and Learning Task

Node classification. We are given a simple, unweighted, undirected and connected graph $G(V, E)$ with $n = |V|$ nodes, $m = |E|$ edges, and no self-loops. Given c classes, $c \geq 2$, each node $i \in V$ hosts a labeled sample (\mathbf{x}_i, y_i) , where \mathbf{x}_i is a feature vector (or set of node attributes or initial embedding) living in some feature space \mathcal{X} , and $y_i \in [c] := \{1, 2, \dots, c\}$ is the class label assigned to node i . In the (transductive) node classification problem, the set of nodes V of G is split into a training set $V_{\text{tr}} \subset V$ and a test set $V_{\text{te}} := V \setminus V_{\text{tr}}$. The learning algorithm is given access to all feature vectors $\mathbf{x}_1, \dots, \mathbf{x}_n$ at the nodes in the graph, as well as the labels y_i of the training nodes $i \in V_{\text{tr}}$. The goal is to maximize accuracy in predicting the labels of nodes in the test set V_{te} .

GNNs. There are several GNN schemes in the literature, from neighborhood aggregation (GraphSAGE, [18]) to spatial convolution (GCN, [24]) to self-attention (GAT, e.g., [33]), and beyond. Yet, the majority of GNN learning schemes can be viewed as performing message passing operations on the feature vectors sitting at each node, followed by feature transformation fed to a suitable activation function. The main idea behind message passing is to iteratively update node representations (feature vectors) by aggregating information from neighboring nodes and passing messages between them. This process helps capture both local and global structural patterns within the graph.

Let d_ℓ be the input dimensionality of the ℓ -th network layer. A GNN message-passing scheme is typically defined as a function that computes a vector $\mathbf{x}_i^{(\ell+1)} \in \mathbb{R}^{d_{\ell+1}}$ for the next layer $\ell + 1$ as:

$$\mathbf{x}_i^{(\ell+1)} \leftarrow \gamma^{(\ell)} \left(\mathbf{x}_i^{(\ell)}, \bigoplus_{j \in \mathcal{N}(i)} \phi^{(\ell)} \left(\mathbf{x}_j^{(\ell)} \right) \right), \quad (1)$$

where $\gamma^{(\ell)}$ is an update function sitting in layer ℓ , $\mathcal{N}(i)$ is the set of nodes in the neighborhood of node i , \bigoplus is a permutation-invariant operator (e.g., maximum, minimum, average, max-pooling, weighted sum, etc.) to aggregate the set of incoming messages from the neighbors of node i , and $\phi^{(\ell)}$ is a message function in layer ℓ . When $\phi^{(\ell)}$, \bigoplus , and $\gamma^{(\ell)}$ are differentiable operators, message-passing layers can be stacked and their parameters can be learned end-to-end via backpropagation. In the above scheme, for each node i , the message function $\phi^{(\ell)}$ computes messages that will be sent to its neighbors $\mathcal{N}(i)$. This function takes into account the features $\mathbf{x}_i^{(\ell)}$ in layer ℓ of the sender node i , the features $\mathbf{x}_j^{(\ell)}$ of the receiving nodes $j \in \mathcal{N}(i)$, and possibly the features of the edges connecting them (although we will not consider problems with edge features here). The message function $\phi^{(\ell)}$ can be implemented as a deep neural network (DNN), and its parameters are typically learned during

training. The update function $\gamma^{(\ell)}$ computes the new node representation $\mathbf{x}_i^{(\ell+1)}$ based on aggregate messages $\phi^{(\ell)}(\mathbf{x}_j^{(\ell)})$, and the previous node representation $\mathbf{x}_i^{(\ell)}$. This function too can be a DNN with learnable parameters.

The above process is repeated for a fixed number of iterations or until a convergence criterion is met. Message passing allows information to propagate through the graph and enables each nodes to capture information from more distant nodes. After the final iteration, a readout function combines the node representations to generate a graph-level representation or output, which can then be used for downstream tasks like node classification.

In particular, a GCN is a special case of (1) where the aggregation of features of neighboring nodes is carried out through a symmetric, left normalized adjacency matrix. This design choice promotes smoothness and robustness in the learned features while preserving the structural properties of the graph. Yet, GCNs rely on a fixed, pre-defined aggregation function, which may limit their ability to model complex relationships between nodes. In contrast, a GAT employs a self-attention mechanism to learn the importance of neighboring nodes in the feature aggregation process. This attention mechanism is adaptive, allowing GATs to weigh neighbors differently based on their relevance to a given node. Consequently, GATs can capture complex relationships and interactions between nodes more effectively than GCNs. The attention mechanism of GATs, however, requires pairwise comparisons between all nodes in the neighborhood, leading to high computational complexity and memory requirements, that hamper their scalability and make them less suitable for real-time applications or deployment on resource-constrained devices.

Effective resistance and graph linearization via random spanning trees. We next introduce our graph linearization procedure, whose goal is to approximately preserve the information contained in the labels of G in the form of its labeling *cutsize* $\Phi(G, y)$, that is, the number of $(i, j) \in E$ such that $y_i \neq y_j$. This is a metric that captures the label complexity⁵ of the node classification problem. A standard inductive bias in this context is the so-called *homophily* principle that essentially posits that strongly connected nodes tend to share the same labels, so that $\Phi(G, y)$ tends to be small on “typical” graphs. A more refined notion of cutsize for node classification that exhibits very appealing properties is the *effective resistance weighted cut-size*

$$\Phi^R(G, y) = \sum_{(i,j) \in E : y_i \neq y_j} r_{i,j},$$

where each edges $(i, j) \in E$ with mismatching labels is weighted according to its *effective resistance* $r_{i,j}$ in G . The effective resistance is a commonly used measure of connectivity (e.g., [26]), since it accounts for both local and global topological properties of the graph at hand. In the interpretation of the graph as an electric network where the edge weights are the edge *conductances* (which are all 1 in our case, as we are considering unweighted graphs only), the effective resistance $r_{i,j}$ between two (non-necessarily adjacent) nodes i and j is the voltage between i and j when a unit current flow is maintained through them. As a quick insight on this measure, one can informally claim that $r_{i,j}$ is small whenever there are many edge-disjoint (and short) paths between i and j , and large otherwise. For instance, if G is a social network, $r_{i,j}$ is roughly inversely proportional to the number $n_{i,j}$ of common friends/connections between users $i, j \in V$ (even if i and j are not directly connected), and it is indeed upper bounded by $\frac{2}{n_{i,j}}$. The largest possible value of $r_{i,j}$ is 1, which corresponds to the case where i and j are adjacent nodes, and (i, j) is a bridge in G , that is, an edge whose removal disconnects G . Hence, $r_{i,j}$ is *locally* density-dependent, in that the contribution of edge (i, j) to $\Phi^R(G, y)$ is small if (i, j) is located in locally dense areas, and is large if (i, j) is located in sparsely connected areas of the graph. The effective resistance $r_{i,j}$ between two adjacent nodes $i, j \in V$ is also equal to the probability that (i, j) belongs to a uniformly generated Random Spanning Tree (RST) T of G (see, e.g., [26]). As a consequence, $\Phi^R(G, y) = \mathbb{E}[\Phi(T, y)]$, the expectation being over the random draw of T . Thus it is also immediate to see that $\Phi^R(G, y) \in [0, n - 1]$. The effective resistance matrix $R = [r_{i,j}]_{i,j=1}^{n \times n}$ is intimately related to the inverse Laplacian matrix of G , and we refer the reader to Appendix A for further background material.

With the above material handy, we are ready to describe how to compress a given (unweighted) graph into a *path graph* (that is, a *list*), together with the invariance properties of this compression. This

⁵We could, in principle, also incorporate feature information, e.g., by considering weighted graphs where the weight $w_{i,j}$ of edge (i, j) is, say, some function of the distance between \mathbf{x}_i and \mathbf{x}_j . We are deliberately avoiding weighted graphs for reasons that will be made clear later on.

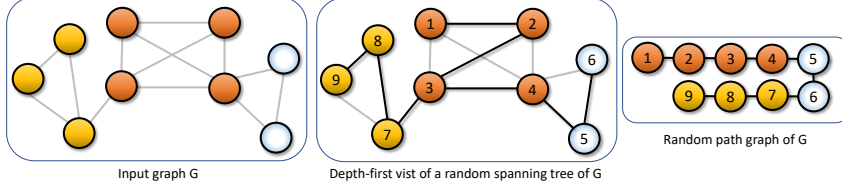


Figure 1: Left: Input graph G with $n = 9$ nodes, each one belonging to one of $c = 3$ possible classes (yellow, orange, and light blue). This example emphasizes homophily: G can be partitioned into 3 uniformly-colored cliques. **Center:** An RST (thick edges) T of G , along with a depth-first visit of T , starting from the top-left orange node. The numbers indicate the visit order. **Right:** An RPG of G computed from the spanning tree T . The linearization in this case produces a path graph that can be split into stretches of uniformly labeled nodes.

material is essentially taken from [5]. The method consists of two steps: (i) drawing a RST T of G and, (ii) generating a path graph P , where the nodes are ordered by a depth-first visit of T , starting from an arbitrary node of V . We call a path graph P so obtained a Random Path Graph (RPG). Figure 1 illustrates this compression procedure through an example.

Note that this graph compression scheme only operates on the graph topology G , that is, it completely disregards the data information (\mathbf{x}_i, y_i) , $i = 1, \dots, n$. Two relevant properties of this graph compression scheme are the following:

(i) **The expected cutsize $\mathbb{E}[\Phi(P, y)]$ of P is at most $2\Phi^R(G, y)$.** This is because, for all labeling y , and all spanning trees T , if P a path graph obtained from T via a depth first visit then $\Phi(P, y) \leq 2\Phi(T, y)$ – see, e.g., [5], Thm. 6 therein. Hence, the loss of information on the labeling y of G due to edge sparsification is at most a factor of 2. Moreover, if the original graph G has areas of tightly connected nodes (as measured by effective resistance) then these nodes tend to be mapped to contiguous stretches of nodes in P , while areas of G that are weakly interconnected will be scattered in P across a few connected sub-paths. Since, by homophily, the dense areas in G tend to belong to the same class, this entails that the contiguous stretches in P will also belong to the same class. See again Figure 1 for an example. This compression technique has been successfully used and analyzed in detail in the literature of transductive online node classification (without features) – see, e.g., [4, 5]. In particular, in [5], the authors show the effectiveness of running a simple 1-Nearest Neighbor (1NN) classification method on the RPG P to predict the labels in the test set. The fact that a simple 1NN method operating on P works so well further strengthens the above intuition about the role played by effective resistance in measuring local graph density. These properties are the cornerstone of GERN.

(ii) **The compression is very fast to compute.** The expected running time for generating P from G is essentially⁶ $\mathcal{O}(n)$, independent of $|E|$ [34]. The linear expected running time only applies to the case where the original graph G is unweighted. This is one of the main reasons why we decided to disregard possible (data-dependent) edge weighting schemes during this preprocessing step.

3 The Proposed GNN Framework

Although our framework is flexible enough to be deployed in several types of GNNs for node classification, in the sequel we just focus on a message passing architectures inspired by the classical Graph Convolutional Networks [24]:

$$\mathbf{x}_i^{(\ell+1)} \leftarrow \gamma^{(\ell)} \left(\mathbf{W}^{(\ell)} \cdot \frac{\sum_{j \in \mathcal{N}(i)} \mathbf{x}_j^{(\ell)}}{|\mathcal{N}(i)|} + \mathbf{B}^{(\ell)} \cdot \mathbf{x}_i^{(\ell)} \right), \quad (2)$$

where $\mathbf{W}^{(\ell)}, \mathbf{B}^{(\ell)} \in \mathbb{R}^{d_{\ell+1} \times d_\ell}$ are learnable parameters, and $\gamma^{(\ell)} : \mathbb{R}^{d_{\ell+1}} \rightarrow \mathbb{R}^{d_{\ell+1}}$ is a vector-wise non-linearity (e.g., a relu activation) that operates on each component separately. The message passing update (2) is executed for k steps, where k is a small constant (a hyperparameter in our experiments). The feature vector at the last layer $\mathbf{x}_i^{(k)}$ is then fed to a standard softmax function to produce one of c possible classes. Training the model weights is carried out by minimizing cross-entropy loss.

GERN, our framework for training a GNN, is summarized in Algorithm 1. It takes as input a graph $G(V, E)$ with n nodes, an unlabeled dataset $\mathbf{x}_1, \dots, \mathbf{x}_n$, where \mathbf{x}_i sits on node $i \in V$, as well as

⁶The linear time complexity holds for “almost” all input graphs, except for pathological cases of very dense and, simultaneously, high diameter graphs (like a so-called lollipop graph) which never occur in practice.

the supervised information y_i contained in the training nodes V_{tr} and the validation set nodes V_{va} . There are two main training parameters, the maximal number of epochs z (that is, the maximal number of gradient descent steps, which also corresponds to the number of RST/RPG generated during training), and the number of hops k , which is the total number of layers of the GNN. The steps can be divided in three phases: Step (1) which can be heavily parallelized as each T_e and P_e can be generated independently for all z epochs; Steps (2,3,4) make up the training step, which are necessary for convergence, and Steps (5,6,7) make the validation, which might be excluded depending on the convergence criterion. The algorithm has one extra ingredient, which we now describe.

RPGs generation via A-RSTs. We generate z RSTs (where z is typically around 100) and linearize them to obtain z RPGs as explained at the end of Section 2. For the sake of efficiency, we adopt a fast hybrid method of RST generation that we call *Approximate RST* (A-RST). An A-RST is a spanning tree that is only an approximate version of a uniformly generated RST. There are two fundamental algorithmic methods to draw a uniformly generated RST. The first one is to include each edge (i, j) of a random walk passing from i to j whenever j is has not been previously visited until $n - 1$ edges have become part of the generated tree. The second method is a faster and more sophisticated method known as the Wilson algorithm [34], which generates an RST by iteratively performing random walks from unvisited nodes selected uniformly at random, deleting loops, and adding the resulting path to the tree. Since the computational bottleneck is the first part for the random walk method and the last part in the Wilson algorithm, we combine the two methods as follows. We first run the random walk method until βn edges are traversed, for some constant $\beta < 1$ (see Appendix D), and then switch to the Wilson algorithm. We also experimentally verified that the probability of including each edge in an A-RST so generated is close to the one achieved by a uniform RST (see Appendix D for details).

Algorithm 1: GERN

Input : $G(V, E)$ with $n = |V|$; features $X = \{x_1, \dots, x_n\}$; labels $y_i, i \in V$; training set $V_{\text{tr}} \subset V$; validation set $V_{\text{va}} \subset V$;
Training parameters: Maximal number of epochs z , number of hops k .
Initialization : Initialize model parameters with random weights (e.g. Glorot).
For each training epoch $e = 1, 2, \dots, z$:
(1) Generate A-RST T_e of G and the corresponding RPG P_e ;
(2) Perform the forward step on $\text{GNN}(X, P_e)$ to calculate the log probabilities of all the labeling classes for each node in the k -hop neighborhood of each node in V_{tr} ;
(3) Compute cross-entropy loss between log probabilities and true classes y_i , for $i \in V_{\text{tr}}$;
(4) Perform a back-propagation step on the training set to update model parameters through the k layers ;
(5) Compute the log probabilities by running $\text{GNN}(\bar{X}, G)$;
(6) Compute cross-entropy loss between log probabilities and true classes y_i , for $i \in V_{\text{va}}$;
(7) **If** [convergence criterion] on validation set satisfied **then** stop.
Test accuracy: Compute accuracy of trained $\text{GNN}(X, G)$ on $V_{\text{te}} = V \setminus V_{\text{tr}}$.

3.1 Understanding the main advantages of GERN

The two main advantages of our GNN approach are: (i) *test-set accuracy*; we outperform other well known GNN baselines on the tested real-world datasets, and (ii) *scalability*, the overall time required to achieve a performance similar (or even superior) to other GNNs' is much lower than those of the tested baselines. We next motivate why these claims are likely to hold in broad scenarios, and not just inspired by a serendipitous outcome of our experiments.

Test set accuracy. A distinctive feature of our GNN training approach is local feature aggregation that incorporates global graph topology information. As illustrated in Section 2, this is achieved by operating on linearized versions of RSTs of the input graph, that retain effective resistance information on the edges. Whereas GERN's local feature aggregation implicitly re-weights the feature vectors of the neighbors of each node, other GNN methods do not consider the network topology at all when computing embeddings on neighborhoods. The re-weighting scheme based on effective resistance is supported by theoretical arguments. In Appendix C we also demonstrate its effectiveness empirically.

Another key feature of GERN is its ability to overcome over-squashing and over-smoothing phenomena, well-known issues limiting GNN performance. This feature is a direct consequence of our handling of the input graph G via RPGs only. While a deeper discussion about how GERN mitigates over-squashing and over-smoothing is given in Appendix B, we here provide illustrative intuitions.

Figure 2(b) depicts the typical bottleneck which generates over-squashing, where the information which the magenta node is passing on to the red node, is influenced by a large number of distant nodes. By operating on a path graph, GERN mitigates this issue, as the degree of each node is at most 2, thus the number of distant nodes influencing the message passing does not grow exponentially with the distance (Figure 2(c)). As for over-smoothing, the benefits of GERN are illustrated in Figure 3, where we see that already at the second layer, the features in the dense GNN (left) tend to concentrate around the average, becoming rapidly indistinguishable, while in the path graph (right) this effect is greatly alleviated.

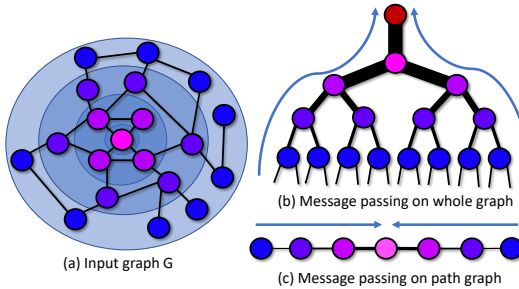


Figure 2: Over-squashing. The input graph, and the typical bottleneck caused by message passing over a large number of distant nodes. Instead, the message passing on a path graph involves far less distant nodes.

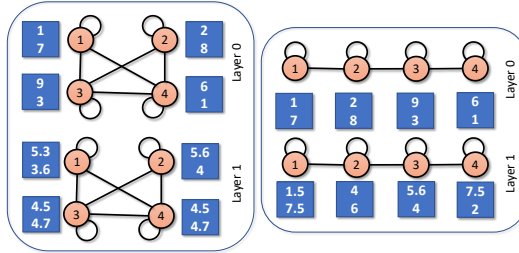


Figure 3: Over-smoothing. Comparison of node embedding updates in a dense GNN (left) vs. a path graph (right), while averaging the feature vectors for each layer (and disregarding for the sake of simplicity weight matrices and non-linearities). The feature vectors in a dense GNN approach the global average (which in this case is $\langle 4.5, 4.7 \rangle$) much faster compared to the path graph.

message passing schemes.

Datasets. Table 1 shows the main statistics of the datasets we used in these experiments. We focus on both small datasets, like Cora and Pubmed, and larger ones, like OGBN-arXiv and AMiner-CS. In the Cora and PubMed graphs, the nodes represent documents while the edges correspond to citation links. Features are document keywords and a class label is associated with each node. The OGBN-arXiv dataset from the Open Graph Benchmark [21] is a directed graph representing the citation network between Computer Science arXiv papers. Nodes come with a 128-dimensional feature vector obtained by averaging the embeddings of words in its title and abstract. AMiner-CS is a citation network based on DBLP [31] where each node corresponds to a paper in Computer Science, and edges represent citation relations between papers. Papers are categorized into 18 topics and feature vectors are obtained by averaging the embeddings of words in its abstract. All directed edges are turned into undirected ones. Self loops are removed.

Scalability. Dealing with path graphs during training brings the obvious benefit that message passing time will be dramatically reduced. The computational price for dealing with path graphs is, of course, the time for generating them. Yet, it is important to observe that the A-RSTs that Algorithm 1 relies upon at each training epoch can be computed *in parallel*, since they are independent of the actual state of the training process (i.e., they do not depend on the weights $\mathbf{W}^{(\ell)}$ and $\mathbf{B}^{(\ell)}$). Overall, this makes the training time per epoch of GERN 10 to 20 times faster than other competing GNN baselines – see Section 4 for details. An empirical study of the extent to which an A-RST approximates a uniformly-generated RST is contained in Appendix D.

By and large, GERN can be viewed as a novel GNN framework for performing randomized pooling operations on sizeable input graphs without compromising accuracy performance.

4 Experiments

In this section, the performance of the proposed framework is evaluated through comparative experiments on popular graph learning benchmarks. We assume that all node features are available for training but only a small portion of labels are known. The small training set regime is meant to emphasize the differences among

Table 1: Datasets statistics.

Dataset	$ V $	$ E $	$ E / V $	c	Features
Cora	2,708	5,429	2.00	7	1,433
Pubmed	19,717	44,338	2.25	3	500
OGBN-arXiv	169,343	2,315,598	13.67	40	128
AMiner-CS	593,486	6,217,004	10.48	18	100

Table 2: Average accuracy and confidence intervals of the various methods under different training conditions. Due to space limitation, the case of training with 10% nodes for Cora and Pubmed is reported in Appendix C.

		10 nodes per class				20 nodes per class				40 nodes per class		1% nodes		5% nodes		20% nodes			
		Cora	Pubmed	Cora	Pubmed	OGBN-arXiv	AMiner-CS	Cora	Pubmed	OGBN-arXiv	AMiner-CS	Cora	Pubmed	OGBN-arXiv	AMiner-CS	Cora	Pubmed	Cora	Pubmed
GRAPHSAINT		77.68 \pm 0.66	73.42 \pm 1.85	80.11 \pm 0.60	78.08 \pm 0.69	46.93 \pm 0.96	52.21 \pm 0.69	81.82 \pm 0.28	80.83 \pm 0.16	55.47 \pm 0.34	53.97 \pm 0.38	80.89 \pm 0.49	85.52 \pm 0.14	68.22 \pm 0.06	63.84 \pm 0.05	86.25 \pm 0.36	87.07 \pm 0.10	85.68 \pm 0.31	87.88 \pm 0.12
GRAPHSAGE		76.24 \pm 0.41	74.36 \pm 1.19	79.55 \pm 0.59	76.07 \pm 0.36	49.50 \pm 0.51	48.72 \pm 0.45	81.64 \pm 0.55	80.15 \pm 0.30	53.76 \pm 0.37	52.88 \pm 0.30	78.85 \pm 0.78	84.48 \pm 0.17	68.54 \pm 0.04	65.36 \pm 0.08	85.17 \pm 0.35	87.05 \pm 0.11	86.17 \pm 0.32	87.14 \pm 0.10
GCN		77.42 \pm 0.69	72.65 \pm 1.68	80.74 \pm 0.56	77.74 \pm 0.75	53.55 \pm 0.43	50.65 \pm 0.50	82.41 \pm 0.49	80.48 \pm 0.22	57.12 \pm 0.18	53.90 \pm 0.37	80.84 \pm 0.53	85.44 \pm 0.09	67.92 \pm 0.05	65.57 \pm 0.02	86.15 \pm 0.32	87.14 \pm 0.10	85.79 \pm 0.24	88.25 \pm 0.10
FGERN-GCN		78.09 \pm 0.52	74.35 \pm 1.11	81.15 \pm 0.33	77.83 \pm 0.68	55.12 \pm 0.35	51.24 \pm 0.55	82.98 \pm 0.40	80.52 \pm 0.21	58.87 \pm 0.18	54.70 \pm 0.36	81.11 \pm 0.38	85.52 \pm 0.14	68.87 \pm 0.05	65.33 \pm 0.04	85.79 \pm 0.24	88.25 \pm 0.10	86.54 \pm 0.21	86.91 \pm 0.07
GERN-SAGE		75.15 \pm 0.64	73.43 \pm 1.06	79.70 \pm 0.31	76.18 \pm 0.57	56.16 \pm 0.45	52.01 \pm 0.47	77.94 \pm 0.62	74.05 \pm 1.19	81.60 \pm 0.51	78.18 \pm 0.57	58.48 \pm 0.35	54.06 \pm 0.41						
GERN-GCN																			

Experimental settings. For Cora and Pubmed, we follow the experimental setup in [35] and [24]. We treat the bag-of-words of the documents as (row-)normalized feature vectors, and we treat citations as (undirected) edges. For training, we randomly sample 20 instances for each class and use them as labeled data. All feature vectors are used for training. We report performance of all models on 10 randomly drawn datasets splits of the same size. The same data splits are used for all methods. We train the model up to a maximal number of training steps (epochs), and select the epoch with highest accuracy on the validation set. Finally we report mean and standard error of prediction accuracy on the test set.

Since training with a fixed number of nodes for each class prevents the models to learn the class prior distribution, we also consider training with a proportion of the nodes selected uniformly at random. For the small datasets (Cora and Pubmed) we consider training sets with 5%, 10% and 20% of nodes, while for larger datasets we consider the smaller fractions of 1% and 5% of training nodes.

For the setting with fixed number of nodes per class, we performed a grid search for best hyperparameters for all models trained with 20 nodes per class, and then used the best values also for 10 and 40 nodes per class. For the setting with fractions of nodes selected for training, we searched for the best hyperparameters at fraction 10% for Cora and Pubmed, and 1% for the others, and then use these hyperparameter values for the remaining cases. We also searched for best number of hidden channels across the values 16, 32, 64, 128, 256, and for best number of layers in the range 2 to 5. Unless otherwise noted, dropout rate was set to 0.5. All hyperparameter values are reported in Appendix C.

We compare our method against the following GNN approaches: a standard Graph Convolutional Network (GCN) [24], GRAPHSAGE [18] and GRAPHSAINT [36]. For our approach, we implement two variants that use RPGs as input with two different GNN architectures, one based on GCN (GERN-GCN), and another one based on GraphSAGE (GERN-SAGE). We also experiment with a method where we use as input the full graph weighted by effective resistance at the edges (FGERN-GCN). For the GERN models that rely on RPGs, we first generate a number of RSTs (250 for Cora and Pubmed, 100 for other datasets) and cycle over them during the training steps.

Training. Unless otherwise noted, we train the models using Adam [23] with learning rate 10^{-2} and weight decay (L2 penalty) $5 \cdot 10^{-4}$, as reported in [24]. The convergence strategy is a piecewise constant learning rate schedule [29] where, if the validation accuracy does not increase for 100 consecutive steps, we reduce the learning rate by a factor of $10^{-0.5}$ until it becomes smaller than 10^{-4} . We train for a maximum of 1.000 training steps each time the learning rate is reduced.

Table 3: Average time (in milliseconds) to perform a training step when fitting OGBN-arXiv data with a training set of 20 nodes per class. The number of hidden channels is 256.

number of layers	2	3	4	5	6
GCN	48.02 \pm 9.51	87.40 \pm 10.73	126.71 \pm 10.81	166.04 \pm 10.69	205.34 \pm 10.07
GERN-GCN	3.50 \pm 6.05	5.04 \pm 5.95	6.62 \pm 5.98	8.45 \pm 5.76	10.58 \pm 5.08

Results. Our results are summarized in Table 2, Table 3, as well as in additional plots and tables in Appendix C. Table 2 shows the test set accuracy of the various methods under the different training conditions. The mean and confidence intervals are measured by 10 repetitions under the same hyperparameters but different training sets (of the same size). Smaller training sizes (e.g., 10 nodes per class) clearly show higher standard error, mostly due to the higher variability in the choice of the training set.

The trend for most datasets is that FGERN-GCN has equal or better performance than GCN, supporting the claim that feature aggregation weighted by effective resistance is a more convenient scheme than flat averaging, which never depreciates the importance of edges that are originally important for the GCN. This phenomenon is particularly pronounced on denser graphs, like OGBN-arXiv, than on sparser ones, like Cora and Pubmed, where RSTs tend to coincide with the original graph (and the usage of effective resistance is less apparent). Moreover, GERN-GCN is either on par or superior to FGERN-GCN, supporting our claim that approximating effective resistance via RPGs is a good strategy to reduce over-squashing and over-smoothing.

Overall, GERN consistently outperforms the competing methods. The only exception to this trend is AMiner-CS with 1% and 5% of training nodes, and our conjecture here is that GERN suffers more when the distribution of classes in the training set is highly unbalanced. AMiner-CS is indeed highly unbalanced in class proportion: the two most common classes (out of 18) make 23% and 14% of the nodes, respectively. As for dependence on the number of layers, the learning curves in Appendix C show that, as the number of layers of the GNN grows, GERN tends to perform better (again corroborating our claim that GERN mitigates over-squashing and over-smoothing), while the GCN shows sign of overfitting. This can be seen from the fact that GERN has a higher training error than the baselines, but better accuracy on the test set. The above is a by-product of our usage of RPGs, which are an extremely sparse version of the input graph, and can be viewed as an ad hoc and implicit regularizer that avoids over-fitting.

Table 3 shows the average time (in milliseconds) for a single training step using both GCN and GERN-GCN on the OGBN-arXiv dataset, with a training set of 20 nodes per class. The trend reported here holds across different datasets and conditions. As expected, execution time increases when increasing the number of GNN layers. The timings reported in Table 3 exclude data loading, A-RSTs generation, and validation set evaluation, focusing solely on the execution of steps 2, 3, and 4 of Algorithm 1. These are the steps directly involved in training. Steps 5, 6, and 7 therein are validation-specific. Step 1 can be parallelized as each A-RST is generated independently from the others: for instance, on the experiment in Table 3, this step takes approximately 10 seconds. The results show that training a GNN using the RPGs is 10-20 times faster than using the full graph.

5 Conclusions, Limitations, and Future Research Directions

In this paper, we have introduced GERN, a novel framework for training GNNs, which improves their scalability and, in most of the settings, increase their accuracy performance. This achievement represents a significant contribution to the domain of graph-based learning. Our approach, solidly rooted in theory, leverages the power of randomization, utilizing path graphs built from random spanning trees, that draw upon topological information of the input graph. We also developed a novel method to approximately generate a random spanning tree very quickly.

The limitations of our investigation are mainly related to the possibility of a more extensive experimental evaluations, involving more datasets and competitors. In particular, it would be significant to assess our framework on graphs denser than the ones used in this paper, where we expect our method to exhibit even further advantages. We also plan a more in-depth quantitative evaluation of GERN’s ability to mitigate over-smoothing (see, e.g., [6]) and over-squashing (see, e.g., [3]). Although our framework is flexible enough to be deployed in several types of GNNs, in this paper we

only combined it with GCN and GraphSAGE: It is surely of interest to extend our investigation by combining GERN with other GNN methods. Finally, through experimental and theoretical analyses, we plan to provide a robust and well-grounded criterion to select the optimal number z of RSTs/RPGs for GERN.

Broader Impact. Our findings have potential implications for a broad range of applications, from social network analysis to computational biology and beyond. Despite the inherent complexity of graph data, our framework offers a compelling solution for efficient and effective GNN training. Our work paves the way for future research in this area so that other researchers can build upon it by combining other neural network algorithms for graph-based learning. Further exploration could extend our methodology to tackle other graph-related challenges or develop similar improvements in other machine learning algorithms. We hope that, through continued research and development, we can push the boundaries of what is possible in graph machine learning more broadly.

As our proposal is a training framework for GNNs, the risks associated with the improper use of our technique are no more than the risks associated with the tools in the existing GNN literature.

References

- [1] Tasweer Ahmad, Lianwen Jin, Luojun Lin, and GuoZhi Tang. Skeleton-based action recognition using sparse spatio-temporal gcn with edge effective resistance. *Neurocomputing*, 423:389–398, 2021.
- [2] Uri Alon and Eran Yahav. On the bottleneck of graph neural networks and its practical implications. In *9th International Conference on Learning Representations, ICLR 2021, Virtual Event, Austria, May 3-7, 2021*. OpenReview.net, 2021.
- [3] Mitchell Black, Amir Nayyeri, Zhengchao Wan, and Yusu Wang. Understanding oversquashing in gnns through the lens of effective resistance. *arXiv preprint arXiv:2302.06835*, 2023.
- [4] Nicolo Cesa-Bianchi, Claudio Gentile, Fabio Vitale, et al. Fast and optimal prediction on a labeled tree. In *COLT 2009: proceedings of the 22nd Annual Conference on Learning Theory, Montréal, Canada, June 18-21, 2009/*, pages 145–156. Omnipress, 2009.
- [5] Nicolo Cesa-Bianchi, Claudio Gentile, Fabio Vitale, and Giovanni Zappella. Random spanning trees and the prediction of weighted graphs. *Journal of Machine Learning Research*, 14(1):1251–1284, 2013.
- [6] Deli Chen, Yankai Lin, Wei Li, Peng Li, Jie Zhou, and Xu Sun. Measuring and relieving the over-smoothing problem for graph neural networks from the topological view. In *Proceedings of the AAAI conference on artificial intelligence*, volume 34, pages 3438–3445, 2020.
- [7] Jianfei Chen, Jun Zhu, and Le Song. Stochastic training of graph convolutional networks with variance reduction. *arXiv preprint arXiv:1710.10568*, 2017.
- [8] Jie Chen, Tengfei Ma, and Cao Xiao. Fastgcn: fast learning with graph convolutional networks via importance sampling. *arXiv preprint arXiv:1801.10247*, 2018.
- [9] Ming Chen, Zhewei Wei, Bolin Ding, Yaliang Li, Ye Yuan, Xiaoyong Du, and Ji-Rong Wen. Scalable graph neural networks via bidirectional propagation. *Advances in neural information processing systems*, 33:14556–14566, 2020.
- [10] Wei-Lin Chiang, Xuanqing Liu, Si Si, Yang Li, Samy Bengio, and Cho-Jui Hsieh. Cluster-gcn: An efficient algorithm for training deep and large graph convolutional networks. In *Proceedings of the 25th ACM SIGKDD international conference on knowledge discovery & data mining*, pages 257–266, 2019.
- [11] Fan RK Chung. *Spectral graph theory*, volume 92. American Mathematical Soc., 1997.
- [12] Chenhui Deng, Zhiqiang Zhao, Yongyu Wang, Zhiru Zhang, and Zhuo Feng. Graphzoom: A multi-level spectral approach for accurate and scalable graph embedding. *arXiv preprint arXiv:1910.02370*, 2019.

[13] Mucong Ding, Tahseen Rabbani, Bang An, Evan Wang, and Furong Huang. Sketch-gnn: Scalable graph neural networks with sublinear training complexity. *Advances in Neural Information Processing Systems*, 35:2930–2943, 2022.

[14] Matthias Fey and Jan Eric Lenssen. Fast graph representation learning with pytorch geometric. *arXiv preprint arXiv:1903.02428*, 2019.

[15] Abderaouf Gacem, Mohammed Haddad, Hamida Seba, Gaetan Berthe, and Michel Habib. Guiding random walks by effective resistance for effective node embedding. In *Pattern Recognition and Artificial Intelligence: Third International Conference, ICPRAI 2022, Paris, France, June 1–3, 2022, Proceedings, Part I*, pages 665–676. Springer, 2022.

[16] Francesco Di Giovanni, Lorenzo Giusti, Federico Barbero, Giulia Luise, Pietro Lio’, and Michael M. Bronstein. On over-squashing in message passing neural networks: The impact of width, depth, and topology. *CoRR*, abs/2302.02941, 2023. doi: 10.48550/arXiv.2302.02941. URL <https://doi.org/10.48550/arXiv.2302.02941>.

[17] Jhony H Giraldo, Fragkiskos D Malliaros, and Thierry Bouwmans. Understanding the relationship between over-smoothing and over-squashing in graph neural networks. *arXiv preprint arXiv:2212.02374*, 2022.

[18] Will Hamilton, Zhitao Ying, and Jure Leskovec. Inductive representation learning on large graphs. *Advances in Neural Information Processing Systems*, pages 1024–1034, 2017.

[19] Mark Herbster and Massimiliano Pontil. Prediction on a graph with a perceptron. *Advances in neural information processing systems*, 19, 2006.

[20] Jeremy G Hoskins, Cameron Musco, Christopher Musco, and Charalampos E Tsourakakis. Learning networks from random walk-based node similarities. *arXiv preprint arXiv:1801.07386*, 2018.

[21] Weihua Hu, Matthias Fey, Marinka Zitnik, Yuxiao Dong, Hongyu Ren, Bowen Liu, Michele Catasta, and Jure Leskovec. Open graph benchmark: Datasets for machine learning on graphs. *Advances in neural information processing systems*, 33:22118–22133, 2020.

[22] Wenbing Huang, Tong Zhang, Yu Rong, and Junzhou Huang. Adaptive sampling towards fast graph representation learning. *Advances in neural information processing systems*, 31, 2018.

[23] Diederik P. Kingma and Jimmy Ba. Adam: A method for stochastic optimization. In Yoshua Bengio and Yann LeCun, editors, *3rd International Conference on Learning Representations, ICLR 2015, San Diego, CA, USA, May 7-9, 2015, Conference Track Proceedings*, 2015. URL <http://arxiv.org/abs/1412.6980>.

[24] Thomas N. Kipf and Max Welling. Semi-supervised classification with graph convolutional networks. In *5th International Conference on Learning Representations, ICLR 2017, Toulon, France, April 24-26, 2017, Conference Track Proceedings*. OpenReview.net, 2017. URL <https://openreview.net/forum?id=BJU4ayYg1>.

[25] Renjie Liao, Marc Brockschmidt, Daniel Tarlow, Alexander L Gaunt, Raquel Urtasun, and Richard Zemel. Graph partition neural networks for semi-supervised classification. *arXiv preprint arXiv:1803.06272*, 2018.

[26] Russell Lyons and Yuval Peres. *Probability on trees and networks*, volume 42. Cambridge University Press, 2017.

[27] Adam Paszke, Sam Gross, Francisco Massa, Adam Lerer, James Bradbury, Gregory Chanan, Trevor Killeen, Zeming Lin, Natalia Gimelshein, Luca Antiga, et al. Pytorch: An imperative style, high-performance deep learning library. *Advances in neural information processing systems*, 32, 2019.

[28] T. Konstantin Rusch, Michael M. Bronstein, and Siddhartha Mishra. A survey on oversmoothing in graph neural networks. *CoRR*, abs/2303.10993, 2023. doi: 10.48550/arXiv.2303.10993. URL <https://doi.org/10.48550/arXiv.2303.10993>.

[29] Leslie N Smith and Nicholay Topin. Super-convergence: Very fast training of neural networks using large learning rates. In *Artificial intelligence and machine learning for multi-domain operations applications*, volume 11006, pages 369–386. SPIE, 2019.

[30] Rakshith S Srinivasa, Cao Xiao, Lucas Glass, Justin Romberg, and Jimeng Sun. Fast graph attention networks using effective resistance based graph sparsification. *arXiv preprint arXiv:2006.08796*, 2020.

[31] Jie Tang, Jing Zhang, Limin Yao, Juanzi Li, Li Zhang, and Zhong Su. Arnetminer: extraction and mining of academic social networks. In *Proceedings of the 14th ACM SIGKDD international conference on Knowledge discovery and data mining*, pages 990–998, 2008.

[32] Jake Topping, Francesco Di Giovanni, Benjamin Paul Chamberlain, Xiaowen Dong, and Michael M. Bronstein. Understanding over-squashing and bottlenecks on graphs via curvature. In *The Tenth International Conference on Learning Representations, ICLR 2022, Virtual Event, April 25-29, 2022*. OpenReview.net, 2022.

[33] Petar Velickovic, Guillem Cucurull, Arantxa Casanova, Adriana Romero, Pietro Lio, Yoshua Bengio, et al. Graph attention networks. *stat*, 1050(20):10–48550, 2017.

[34] David Bruce Wilson. Generating random spanning trees more quickly than the cover time. In *Proceedings of the twenty-eighth annual ACM symposium on Theory of computing*, pages 296–303, 1996.

[35] Zhilin Yang, William Cohen, and Ruslan Salakhudinov. Revisiting semi-supervised learning with graph embeddings. In *International conference on machine learning*, pages 40–48. PMLR, 2016.

[36] Hanqing Zeng, Hongkuan Zhou, Ajitesh Srivastava, Rajgopal Kannan, and Viktor Prasanna. Graphsaint: Graph sampling based inductive learning method. *arXiv preprint arXiv:1907.04931*, 2019.

[37] Zhiqiang Zhao and Zhuo Feng. Effective-resistance preserving spectral reduction of graphs. In *Proceedings of the 56th Annual Design Automation Conference 2019*, pages 1–6, 2019.

A Further Background Material on Effective Resistance

As discussed in Section 2, a key notion at the basis of our sparsification process is that of effective resistance, which is intimately related to the inverse Laplacian matrix of G . We next provide a number of *equivalent* ways of formally defining the effective resistance $r_{i,j}$ between two adjacent nodes i and j . The equivalence of these definitions is often exploited for the design of a graph-based learning algorithm to solve problems where homophily is the basic inductive principle.

- $r_{i,j}$ can be computed by applying the so called *series* and *parallel* laws of electrical networks (see, e.g., [26]).
- In an unweighted graph G , $r_{i,j}$ is equal to the probability that (i, j) belongs to a uniformly generated random spanning tree (RST) T . —see, e.g., [26]. Hence, $\Phi^R(G, y)$ is equal to the expected number of edges with mismatching labels that happen to be included in T , the expectation being over the generation of T . It is therefore also immediate to see why $\Phi^R(G, y) \in [0, n - 1]$.
- $r_{i,j}$ can also be related to random walk in G since an RST can be generated by using the following method: Start a random walk from an arbitrary node, including all traversed edges except the ones which create a cycle with the previously included edges, until all nodes in V are visited. The probability that such a random walk includes edge $(i, j) \in E$ is equal to $r_{i,j}$.
- $r_{i,j}$ can also be expressed in terms of the pseudoinverse of the *Laplacian matrix* L of G . The Laplacian matrix L can be written as

$$L = D - A ,$$

where D is the diagonal matrix containing in its i -th diagonal entry the degree of node i in G , and A is the adjacency matrix of G . Given L 's pseudoinverse $L^\dagger = [L_{i,j}^\dagger]_{i,j=1}^{n \times n}$ we have, for each $(i, j) \in E$,

$$r_{i,j} = (\mathbf{e}_i - \mathbf{e}_j)^\top L^\dagger (\mathbf{e}_i - \mathbf{e}_j) = L_{i,i}^\dagger + L_{j,j}^\dagger - 2L_{i,j}^\dagger,$$

where \mathbf{e}_i is the i -th vector in the canonical basis of \mathbb{R}^n .

B Discussion on Over-squashing and Over-smoothing

As briefly discussed in Section 3.1, the intrinsic sparsity of the path graphs at the basis of GERN provides, as a very interesting side-effect, the capability of greatly mitigating the effects of over-squashing and over-smoothing. We now give further insights on how GERN manages to avoid over-squashing and over-smoothing.

First, GERN only operates on path graphs derived from RSTs of G , hence we simultaneously alleviate both issues. Because our method aggregates at each node only information located k hops away (where k is typically a small constant), and the degree of each node on an RPG is at most 2, no bottleneck is likely to cause over-squashing when trying to capture long-range interactions. This is illustrated in Figure 2 (main body of the paper), where we compare the message dynamics of a relatively dense graph to that of a path graph.

For the very same reason, provided the RPG representation is an accurate representation of the original graph G , our method is likely to avoid the loss of discriminative power in node representations due to over-smoothing. This can be coarsely illustrated by resorting to an analogy with the convergence properties of a random walk (ergodic Markov Chain) to its stationary distribution. A GNNs operates by iteratively applying a neighborhood aggregation scheme, where each node's representation is updated based on the representations of its neighbors. When we consider a random walk on a graph, each step moves from the current node to a randomly chosen neighbor. The random walk transition matrix characterizes the probabilities of these transitions. The process of information propagation in GNNs is somewhat similar to a random walk on the graph. Each layer in the GNN can be seen as a step in a random walk. As more layers (i.e., steps in the random walk) are applied, the node representations converge towards a homogeneous representation, causing the nodes to lose their unique characteristics. This is akin to the behavior of a random walk over many steps, where the current location becomes increasingly independent of the starting location, as the random walk tends towards its stationary distribution. This applies specifically to undirected (and connected) graphs, where the corresponding Markov chain is known to be ergodic. Figure 3 (main body of the paper) contains a simple illustration.

The weight matrices $\mathbf{W}^{(\ell)}$ and $\mathbf{B}^{(\ell)}$ learned during the training process of a GCN in Eq. (2) define the transformations applied to the aggregate features from neighboring nodes. These weights shape how node representations evolve across layers of the GNN and, consequently, they have a wide impact on over-smoothing. The weights determine how information is aggregated from neighboring nodes, which is conceptually similar to the transitioning across nodes in a random walk. However, in a simple random walk, the transition probabilities are fixed (typically based on the graph's structure), while in a GCN, the weight matrices are learned.

One source of inspiration comes from the recent paper [17], where the authors view over-smoothing on a given graph topology as the result of repeatedly applying a random walk transition matrix to a node feature, which eventually leads to a stationary distribution, thus washing away all feature information. A random walk on a path-like graph will hardly approximate the stationary state if we constrain the number of hops k to be a small number. This may not be the case if we operate on a graph with a smaller diameter.

Specifically, given a simple connected graph $G(V, E)$, with node degrees d_1, d_2, \dots, d_n , the random walk transition matrix (left normalized adjacency matrix) is defined as $P := D^{-1}A$, where A is the adjacency matrix of G , and D is a diagonal matrix such that $D_{i,i} := d_i$. Let G' be the graph built from G by adding one self-loop edge with weight d_i for each edge $i \in V$. Note that G' can be viewed as the graph used by GERN when aggregating the information on an RPG (if we disregard the weight matrices which change over time), since the self-loop weight is at most twice the weight of the other edges in G . [17] builds on the standard spectral theory of Markov Chains [11] (Eq. 1.14, p. 15),

where the authors provide a lower bound for the number of steps s of an (ergodic) random walk on G' with any initial distribution $f : V \rightarrow \mathbb{R}$ with $\sum_i f(i) = 1$, such that the Euclidean distance $\epsilon(s) = \|\mathbf{f}P^s - \boldsymbol{\pi}\|_2$ from the stationary distribution $\boldsymbol{\pi}$ is at most $\epsilon(s)$. More precisely, they prove the bound

$$\epsilon(s) \leq \frac{\max_i \sqrt{d_i}}{\min_j \sqrt{d_j}} \exp\left(-s \frac{\lambda_1}{2}\right),$$

where λ_1 is the smallest non-null eigenvalue of the symmetrically normalized Laplacian matrix of G . In the case of a RPG, we have $\frac{\max_i \sqrt{d_i}}{\min_j \sqrt{d_j}} = \Theta(1)$, and $\lambda_1 = 2 - 2 \cos\left(\frac{\pi}{n+1}\right) = \frac{2\pi^2}{n^2} + \mathcal{O}\left(\frac{1}{n^2}\right)$, for $n \rightarrow \infty$. In order to have $\epsilon(s) \leq \epsilon$ we then need to have $s = \Omega\left(\frac{2n^2}{\pi^2} \log\left(\frac{\sqrt{2}}{\epsilon}\right)\right)$, that is, for any approximation level $\epsilon > 0$, the number of GNN layers has to be $\Omega(n^2)$.

Since in GERN, for each RPG, the GNN has only $k \ll n$ layers, this gives a good indication that, under the above-described analogy with random walks, we largely mitigate over-smoothing phenomena during training.

C Further Experimental Results

This appendix reports the whole set of experimental results. Table 4 and Table 5 have the same content as Table 2 from the main body, where we added the missing entries. Figure 4 and 5 contain relevant comparisons of learning curves on both training and test set across different algorithms. Table 6 contains the hyperparameter configurations we used to achieve the results contained in Tables 4 and 5.

Table 4: Average accuracy and confidence intervals of the various methods under different training conditions for the two datasets Cora and Pubmed.

	# nodes per class	Cora	Pubmed	Train prop.	Cora	Pubmed
GraphSAINT	10	77.68 \pm 0.66	73.42 \pm 1.85	5%	80.89 \pm 0.49	85.52 \pm 0.14
GraphSAGE		76.24 \pm 0.41	74.36 \pm 1.19		78.85 \pm 0.78	84.48 \pm 0.17
GCN		77.42 \pm 0.69	72.65 \pm 1.68		80.84 \pm 0.53	85.44 \pm 0.09
FGERN-GCN		78.09 \pm 0.52	74.35 \pm 1.11		81.11 \pm 0.38	85.52 \pm 0.14
GERN-SAGE		75.15 \pm 0.64	73.43 \pm 1.06		78.72 \pm 0.69	85.52 \pm 0.17
GERN-GCN		77.94 \pm 0.62	74.05 \pm 1.19		81.57 \pm 0.52	85.67 \pm 0.14
GraphSAINT	20	80.11 \pm 0.60	78.08 \pm 0.69	10%	84.02 \pm 0.28	86.43 \pm 0.12
GraphSAGE		79.55 \pm 0.59	76.07 \pm 0.36		83.00 \pm 0.31	86.41 \pm 0.12
GCN		80.74 \pm 0.56	77.74 \pm 0.75		83.95 \pm 0.32	86.56 \pm 0.11
FGERN-GCN		81.15 \pm 0.33	77.83 \pm 0.68		83.92 \pm 0.35	86.57 \pm 0.13
GERN-SAGE		79.70 \pm 0.31	76.18 \pm 0.57		82.87 \pm 0.37	87.11 \pm 0.08
GERN-GCN		81.60 \pm 0.51	78.18 \pm 0.57		84.51 \pm 0.31	86.49 \pm 0.07
GraphSAINT	40	81.82 \pm 0.28	80.83 \pm 0.16	20%	86.25 \pm 0.36	87.07 \pm 0.10
GraphSAGE		81.64 \pm 0.55	80.15 \pm 0.30		85.68 \pm 0.31	87.88 \pm 0.12
GCN		82.41 \pm 0.49	80.48 \pm 0.22		86.17 \pm 0.35	87.05 \pm 0.11
FGERN-GCN		82.98 \pm 0.40	80.52 \pm 0.21		86.15 \pm 0.32	87.14 \pm 0.10
GERN-SAGE		81.90 \pm 0.39	78.59 \pm 0.35		85.79 \pm 0.24	88.25 \pm 0.10
GERN-GCN		82.86 \pm 0.41	81.02 \pm 0.18		86.54 \pm 0.21	86.91 \pm 0.07

The experiments were primarily executed utilizing two open-source Python libraries: PyTorch [27] and PyTorch Geometric [14]. PyTorch was instrumental in automating the process of differentiation, while PyTorch Geometric facilitated our work with graph datasets.

Figures 4 and 5 show the progress of train accuracy, test accuracy, train loss and test loss when training different models using the OGBN-arXiv dataset with a training set of 20 nodes per class. The models have a fixed number of 256 hidden channels, and in each column we show the progress of the models with increasing number of layers (2,3,4,5 and 6). In Figure 4 we compare the curves of two methods that are based on the GCN architecture (GCN and GERN-GCN) while in Figure 5 we compare the curves of two methods based on SAGE (GraphSAGE and GERN-SAGE). In this specific

Table 5: Average accuracy and confidence intervals of the various methods under different training conditions for the two datasets OGBN-ArXiv and AMiner-CS.

	# nodes per class	OGBN-arXiv	AMiner-CS	Train prop.	OGBN-arXiv	AMiner-CS
GraphSAINT	20	46.93 \pm 0.96	52.21 \pm 0.69	1%	60.11 \pm 0.20	62.93 \pm 0.09
GraphSAGE		49.50 \pm 0.51	48.72 \pm 0.45		62.36 \pm 0.14	63.96 \pm 0.08
GCN		53.55 \pm 0.43	50.65 \pm 0.50		65.13 \pm 0.11	64.48 \pm 0.04
FGERN-GCN		55.12 \pm 0.35	51.24 \pm 0.55		65.01 \pm 0.09	64.46 \pm 0.06
GERN-SAGE		56.16 \pm 0.45	52.01 \pm 0.47		64.49 \pm 0.14	62.88 \pm 0.07
GERN-GCN		58.48 \pm 0.35	54.06 \pm 0.41		65.91 \pm 0.10	63.03 \pm 0.05
GraphSAINT	40	55.47 \pm 0.34	53.97 \pm 0.38	5%	68.22 \pm 0.06	63.84 \pm 0.05
GraphSAGE		53.76 \pm 0.37	52.88 \pm 0.30		68.54 \pm 0.04	65.36 \pm 0.08
GCN		57.12 \pm 0.18	53.90 \pm 0.37		67.92 \pm 0.05	65.57 \pm 0.02
FGERN-GCN		58.87 \pm 0.18	54.70 \pm 0.36		68.87 \pm 0.05	65.33 \pm 0.04
GERN-SAGE		57.00 \pm 0.39	56.28 \pm 0.24		68.65 \pm 0.07	63.29 \pm 0.04
GERN-GCN		61.84 \pm 0.33	55.91 \pm 0.30		68.25 \pm 0.06	63.32 \pm 0.05

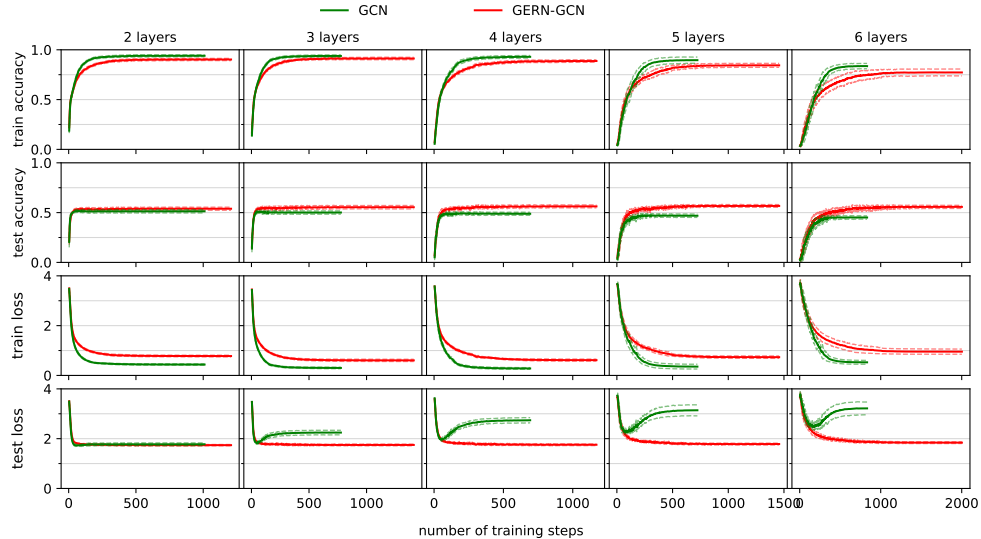


Figure 4: Learning curves, from first to last row: train accuracy, test accuracy, train loss, test loss. Red is GERN-GCN, green is GCN. The number of hidden channels is set to 256. Curves are the average over 10 runs.

setting, the model that performs better is GERN-GCN (see Table 5) with 5 layers and 256 hidden channels (see Table 6). In Figure 4 we compare GERN-GCN with its counterpart that takes as input the full graph (GCN). The best configuration for GCN is 3 layers and 256 channels. It is clear that GCN suffers of overfitting when the number of layers increase, while GERN-GCN is less susceptible to overfitting with a higher number of layers. The same trend can be seen when comparing the other two models with the same GNN architecture (GraphSAGE and GERN-SAGE), even though this is not the best performing architecture in this setting. Finally, the curves show that even though GERN models take a higher number of epochs than their counterparts to converge, this number is not much higher, and considering that training steps with GERN are almost an order of magnitude faster, the whole training process is still much faster than their counterparts.

D Experimental validation of A-RSTs

We compared different ways of generating (random) spanning trees. We used the standard Wilson algorithm [34] (the resulting trees will simply be called RST), our A-RST method from Section 3 in the main body, and a third randomized method based on Breadth-First Search (BFS), where the root

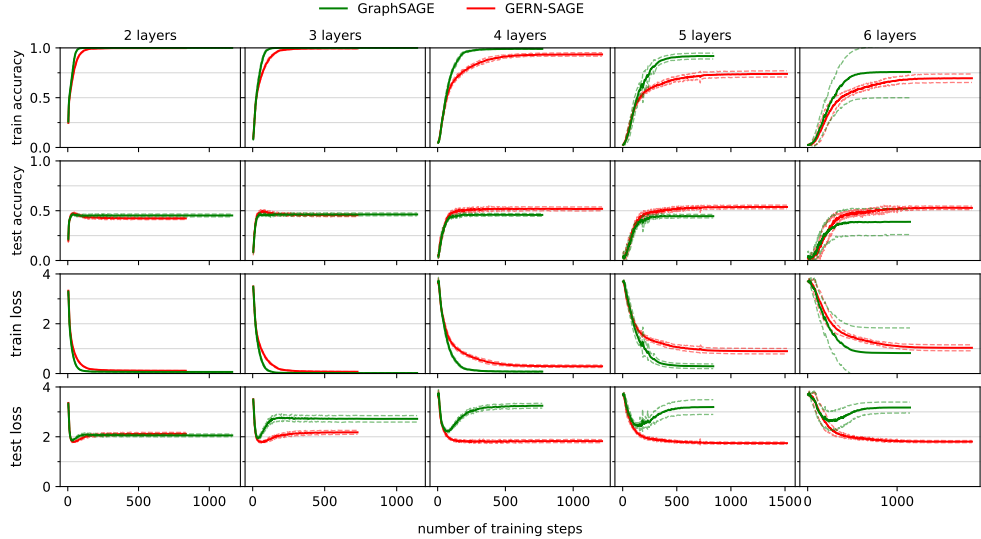


Figure 5: Learning curves, from first to last row: train accuracy, test accuracy, train loss, test loss. Red is GERN-SAGE, green is GraphSAGE. The number of hidden channels is set to 256. Curves are the average over 10 runs.

Table 6: Hyperparameter configurations (number of layers and number of hidden channels) used to achieve the accuracy scores in Tables 4 and 5. The parameters that turned out to be best for 20 nodes per class were used also for 10 and 40 nodes per class. The parameters that turned out to be best for fractions of 10% and 1% were used also for the other fractions.

	Cora	PubMed	OGBN-arXiv	Aminer-CS	Cora 10%	PubMed 10%	OGBN-arXiv 1%	Aminer-CS 1%
	20 nodes per class							
GraphSAINT	3 - 356	4 - 256	4 - 256	3 - 32	2 - 16	2 - 64	3 - 256	4 - 64
GraphSAGE	3 - 256	4 - 256	4 - 256	3 - 32	2 - 16	2 - 64	3 - 256	4 - 64
GCN	3 - 128	2 - 256	3 - 256	3 - 64	2 - 256	2 - 64	2 - 128	4 - 64
FGERN-GCN	3 - 128	2 - 256	3 - 256	3 - 64	2 - 256	2 - 64	3 - 256	4 - 64
GERN-SAGE	3 - 128	4 - 128	6 - 128	4 - 64	2 - 16	2 - 32	6 - 128	3 - 64
GERN-GCN	3 - 128	2 - 256	5 - 256	3 - 64	2 - 256	2 - 128	3 - 256	4 - 64

is selected at random and the neighbors of nodes are visited in random order. For each method, we generated N spanning trees, where $N = 1000$ for Cora and Pubmed, and $N = 500$ for OGBN-arXiv and AMiner-CS. Next, we calculated the probabilities and associated standard error for each edge in E . Then we calculated the absolute differences between the probability of including each edge with A-RST and RST, and between BFS and RST. Table 7 shows the average of the absolute differences across all edges in E . It shows that the average probability difference is close to 1% for A-RST, while the difference when using BFS varies for each dataset, and is more than three times larger in OGBN-arXiv and AMiner-CS. For Cora and PubMed, BFS produces closer probabilities due to their sparsity. Furthermore, the fraction of edges that are not included neither in the A-RSTs nor in the RSTs is in the order of 10^{-4} , which is a good indicator that N is chosen large enough to measure how good an A-RST approximates an RST.

Figure 6 displays histograms indicating the frequency of probability values across all edges in the OGBN-arXiv dataset, derived from RST, A-RST, and BFS methods. Each histogram represents the normalized frequency of edges with their probability of being included in the 500 spanning trees generated via each respective method. A difference can be observed between the histograms from RST and BFS, but RST and A-RST appear quite similar visually. To support this observation, we carried out a Kolmogorov-Smirnov test to evaluate the equality of distributions, comparing the histograms for all datasets (results displayed in Table 8). When comparing the histograms from RST and A-RST, the high p-values suggest that we cannot exclude that the values are drawn from the same distribution. On the other hand, the comparison between RST and BFS histograms yields small p-values, indicating a significant likelihood that the samples are drawn from different distributions.

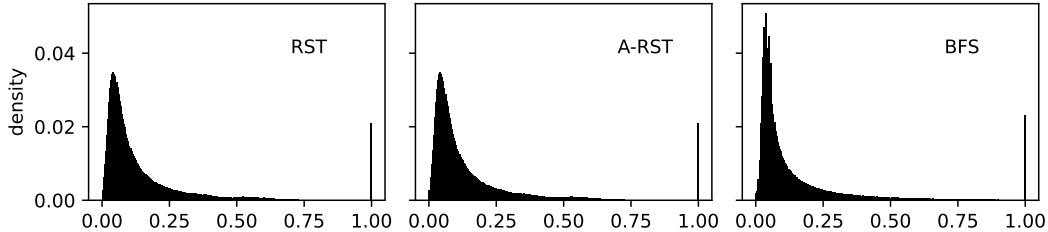


Figure 6: Histograms with the relative frequency of probability values assigned to edges in the OGBN-arXiv dataset using three different spanning tree generation methods.

Table 7: Average of the absolute differences between the probability of including each edge with A-RST and RST, and between BFS and RST.

	Cora	PubMed	OGBN-arXiv	Aminer-CS
A-RST vs. RST	0.0153 ± 0.0130	0.0116 ± 0.0088	0.0142 ± 0.0082	0.0170 ± 0.0111
BFS vs. RST	0.1232 ± 0.0123	0.0574 ± 0.0086	0.0472 ± 0.0079	0.0571 ± 0.0108

Table 8: Kolmogorov-Smirnov test of the equality of distributions between the probability value histograms of A-RST vs. RST, and with BFS vs. RST. In brackets we report the p-value of each test.

	Cora	PubMed	OGBN-arXiv	Aminer-CS
A-RST vs. RST	0.008 (0.87)	0.002 (0.97)	0.0005 (0.95)	0.002 (0.97)
BFS vs. RST	$0.1 (< 10^{-8})$	$0.043 (< 10^{-8})$	$0.091 (< 10^{-8})$	$0.076 (< 10^{-8})$